Article

THE EMBO JOURNAL

Space exploration by dendritic cells requires maintenance of myosin II activity by IP$_3$ receptor 1

Paola Solanes[1], Mélina L Heuzé[1,†], Mathieu Maurin[1,†], Marine Bretou[1], Franziska Lautenschlaeger[2], Paolo Maiuri[2], Emmanuel Terriac[2], Maria-Isabel Thoulouze[3], Pierre Launay[4], Matthieu Piel[2], Pablo Vargas[1,*] & Ana-Maria Lennon-Duménil[1,**]

Abstract

Dendritic cells (DCs) patrol the interstitial space of peripheral tissues. The mechanisms that regulate their migration in such constrained environment remain unknown. We here investigated the role of calcium in immature DCs migrating in confinement. We found that they displayed calcium oscillations that were independent of extracellular calcium and more frequently observed in DCs undergoing strong speed fluctuations. In these cells, calcium spikes were associated with fast motility phases. IP$_3$ receptors (IP$_3$Rs) channels, which allow calcium release from the endoplasmic reticulum, were identified as required for immature DCs to migrate at fast speed. The IP$_3$R1 isoform was further shown to specifically regulate the locomotion persistence of immature DCs, that is, their capacity to maintain directional migration. This function of IP$_3$R1 results from its ability to control the phosphorylation levels of myosin II regulatory light chain (MLC) and the back/front polarization of the motor protein. We propose that by upholding myosin II activity, constitutive calcium release from the ER through IP$_3$R1 maintains DC polarity during migration in confinement, facilitating the exploration of their environment.

Introduction

Dendritic cells (DCs) present antigens onto MHC molecules to T lymphocytes and are therefore strictly required for the initiation of adaptive immune responses. Immature DCs are found in most peripheral tissues, where they patrol their environment by internalizing extracellular antigens. Although in some tissues DCs appear to be rather sessile, patrolling of the ear skin and of the gut was shown to be associated with sustained DC migration (Ng *et al*, 2008; Tal *et al*, 2011; Lelouard *et al*, 2012). Whether these differences are due to tissue-intrinsic properties, to the involvement of distinct DC subsets, or result from tissue manipulation during experimentation is unclear. Nonetheless, the capacity of DCs to migrate in the confined environment of peripheral tissues is likely to be essential for them to efficiently carry out their immune sentinel function.

The molecular mechanisms that control DC migration have started to be addressed. Mature DCs, which are in charge of transporting antigens to lymph nodes for presentation to T cells, do not need integrin-based adhesion to migrate in 3-dimensional (3D) environments. Indeed, these cells can migrate by the force of actin polymerization at the leading edge, while the contraction of their rear by myosin II allows nucleus transport through narrow gaps (Lammermann *et al*, 2008; Renkawitz *et al*, 2009). Less is known on the mechanisms that control the migration of immature DCs. This is mainly due to the fact that (i) intra-vital imaging does not provide enough resolution to analyze intracellular protein dynamics in DCs migrating *in vivo*, (ii) immature DCs purified from peripheral tissues rapidly become activated in culture and therefore cannot be used for mRNA silencing and cell biological studies, and (iii) bone marrow-derived DCs, which maintain their immature phenotype *in vivo*, migrate poorly when plated on 2D surfaces. To circumvent these problems, we have built 1D (micro-channels) and 2D micro-fabricated devices that mimic the interstitial space of peripheral tissues to unravel the cell biological mechanisms involved in the migration of bone marrow-derived immature DCs. Using these tools, we showed that immature DC fast migration is facilitated by cell confinement and requires myosin II activity (Faure-Andre *et al*, 2008; Heuze *et al*, 2013). In addition, we observed that immature DCs migrating in confined micro-channels display important velocity fluctuations, alternating between fast and slow motility phases (Faure-Andre *et al*, 2008). Whether and how velocity fluctuations

1 Inserm-U932, Institut Curie, Paris, France
2 CNRS-UMR144, Institut Curie, Paris, France
3 Unité de Virologie Structurale, CNRS-UMR3469, Institut Pasteur, Paris, France
4 Faculté de Médecine X. Bichat, Inserm-U1149, Paris, France
   *Corresponding author. Tel: +33 1 56 24 63 83; Fax: +33 1 56 24 63 19; E-mail: pablo.vargas@curie.fr
   **Corresponding author. Tel: +33 1 56 24 64 27; Fax: +33 1 56 24 64 38; E-mail: amlennon@curie.fr
   †Equal contribution by alphabetical order

are regulated during DC migration in confinement is the aim of the present study.

Calcium (Ca^{2+}) is a ubiquitous intracellular signal that controls cell polarity and migration although the effector mechanisms involved are not fully understood (Brundage et al, 1991). Front-to-back Ca^{2+} gradients have been observed within cells migrating on 2D substrates and proposed to promote traction stress distribution and front/back coupling for persistent locomotion (Brundage et al, 1991; Lee et al, 1999). Recently, local Ca^{2+} increments named "Ca^{2+} flickers" were identified at the leading edge of keratocytes migrating in 2D as involved in directional migration in response to chemokine gradients (Wei et al, 2009, 2012). Their formation relies on the activity of the stretch-activated Ca^{2+} channel TRPM7 that triggers intracellular Ca^{2+} release from the endoplasmic reticulum (ER) through IP_3 receptor (IP_3R) channels as well as on myosin II activity. In addition, discrete Ca^{2+} pulses were shown to induce local lamellipodia retraction at the front of endothelial cells migrating on 2D surfaces (Tsai & Meyer, 2012). Lamellipodia retraction results from the activation of the Ca^{2+}/calmodulin-dependent myosin light chain (MLC) kinase (MLCK) that phosphorylates MLC and thereby triggers local actin contraction. However, the role of intracellular calcium dynamics in cells migrating in confinement has not been addressed.

In DCs, the role of Ca^{2+} signaling has mainly been investigated in the context of chemotaxis, implicating the activation of G-coupled receptors through the $PtdIns(4,5)P_2$ (PIP_2)/phospholipase C(PLC) pathway and the surface molecule CD38 (Lee, 2001; Partida-Sanchez et al, 2004). The Ca^{2+}-activated non-selective channel TRPM4 and the lysosomal Ca^{2+} channel TRPM2 were also highlighted as essential for chemokine-dependent migration of activated DCs (Barbet et al, 2008; Guinamard et al, 2010; Knowles et al, 2013). However, whether and how Ca^{2+} intracellular stores regulate the homeostatic migration of immature DCs in the context of tissue patrolling has not been investigated so far.

Here, we analyzed the role of Ca^{2+} signaling in immature DC migration in confinement. We observed that speed-fluctuating DCs exhibited intracellular Ca^{2+} fluctuations that were associated with fast motility phases and did not rely on extracellular Ca^{2+} influx. IP_3Rs were found to be required for maintenance of intracellular Ca^{2+} levels and fast locomotion of immature DCs. We further identified IP_3R1 as a specific regulator of their speed fluctuations and migration persistence. IP_3R1 maintains the intracellular gradient of myosin II in migrating DCs, allowing efficient space exploration. IP_3R1 and ER Ca^{2+} stores therefore emerge as key regulators of sustained myosin II activity and polarity in amoeboid-like confined cell migration.

Results

Ca^{2+} oscillations are predominantly observed in immature DCs that undergo significant speed fluctuations and changes of direction

We aimed at unraveling the role of Ca^{2+} signaling in migration of immature DCs evolving in a confined environment. To address

this question, we monitored intracellular Ca^{2+} dynamics in mouse bone marrow-derived DCs migrating in fibronectin-coated 5×5 μm micro-fabricated channels. Although it is not clear to which DC subset these cells correspond to, they provide a unique model to analyze molecular mechanisms that can be addressed neither in vivo nor in tissue-isolated DCs. Beyond mimicking the confined space of tissues, micro-channels are compatible with high-resolution time-lapse microscopy and further impose to DCs an elongated well-defined shape that facilitates mechanistic studies (Supplementary Fig S1A) (Faure-Andre et al, 2008; Heuze et al, 2011). Analysis of cytosolic Ca^{2+} dynamics in immature DCs loaded with the Ca^{2+} dye Oregon Green BAPTA showed that intracellular Ca^{2+} spikes were observed in ~70% of migrating cells although at variable frequencies (n = 45, examples on Fig 1A and Supplementary Videos S1 and S2). Surprisingly, neither the percentage of cells displaying Ca^{2+} spikes nor spike frequency were significantly affected when adding extracellular BAPTA (71% ± 11 versus 55% ± 7, n = 67 and Supplementary Fig S1B), even though Ca^{2+} influx into DCs was abolished in the presence of this extracellular Ca^{2+} chelator (Supplementary Fig S1C). These data indicate that the intracellular Ca^{2+} fluctuations observed in migrating DCs do not result from extracellular Ca^{2+} influx but rather from Ca^{2+} released from intracellular stores. Accordingly, we found that chelation of extracellular Ca^{2+} did not impair immature DC migration in micro-channels, collagen-coated transwells, or collagen gels (Fig 1B, Supplementary Fig S1D and E). Noticeably, the migration of T lymphocytes in micro-channels was strongly altered by addition of BAPTA into the milieu (Fig 1C), indicating that the ability to move independently of extracellular Ca^{2+} does not apply to all leukocytes but might rather represent a peculiarity of DCs.

To investigate whether these intracellular Ca^{2+} oscillations play a role in DC migration, we monitored the mean Ca^{2+} activity, that is, the area under the Ca^{2+} fluctuation curve (Ca^{2+} $\Delta F/F_0$ versus time, Fig 1A), together with cell speed. We did not detect a strong correlation between the amount of released Ca^{2+} and the mean speed of DCs (Supplementary Fig S2A). However, significant mean Ca^{2+} activities ($\Delta F/F_0 > 0.1$) were almost exclusively detected in DCs migrating at fast speed (mean speed > 5 μm/min) (Supplementary Fig S2A). This was observed in both fibronectin and PEG-coated micro-channels (Supplementary Fig S2B), indicating that neither Ca^{2+} oscillations nor DC velocity require the engagement of integrins.

Noticeably, we found that among fast-migrating DCs, cells undergoing significant velocity fluctuations during locomotion (instantaneous speed variance > 30% of the mean speed, Supplementary Fig S2C) exhibited increased levels of cytosolic Ca^{2+} (Fig 1D). Supporting this result, we observed that addition of the chemokine CCL3, known to act on immature DCs (Sallusto et al, 1998), significantly increased both their speed fluctuations (Fig 1E and $\Delta V/V_0 > 0.3$ in 72% of control versus 85% of CCL3-treated DCs) and mean Ca^{2+} activity (Fig 1F). However, CCL3 did not compromise the migration speed of DCs nor induce their maturation (Supplementary Fig S2D and E). Noticeably, in speed-fluctuating DCs, Ca^{2+} release was predominantly associated with fast motility phases as compared to slow motility ones (Fig 1A (upper panel) and G, and Supplementary Fig S2F). This association was observed in DCs that maintained their direction after
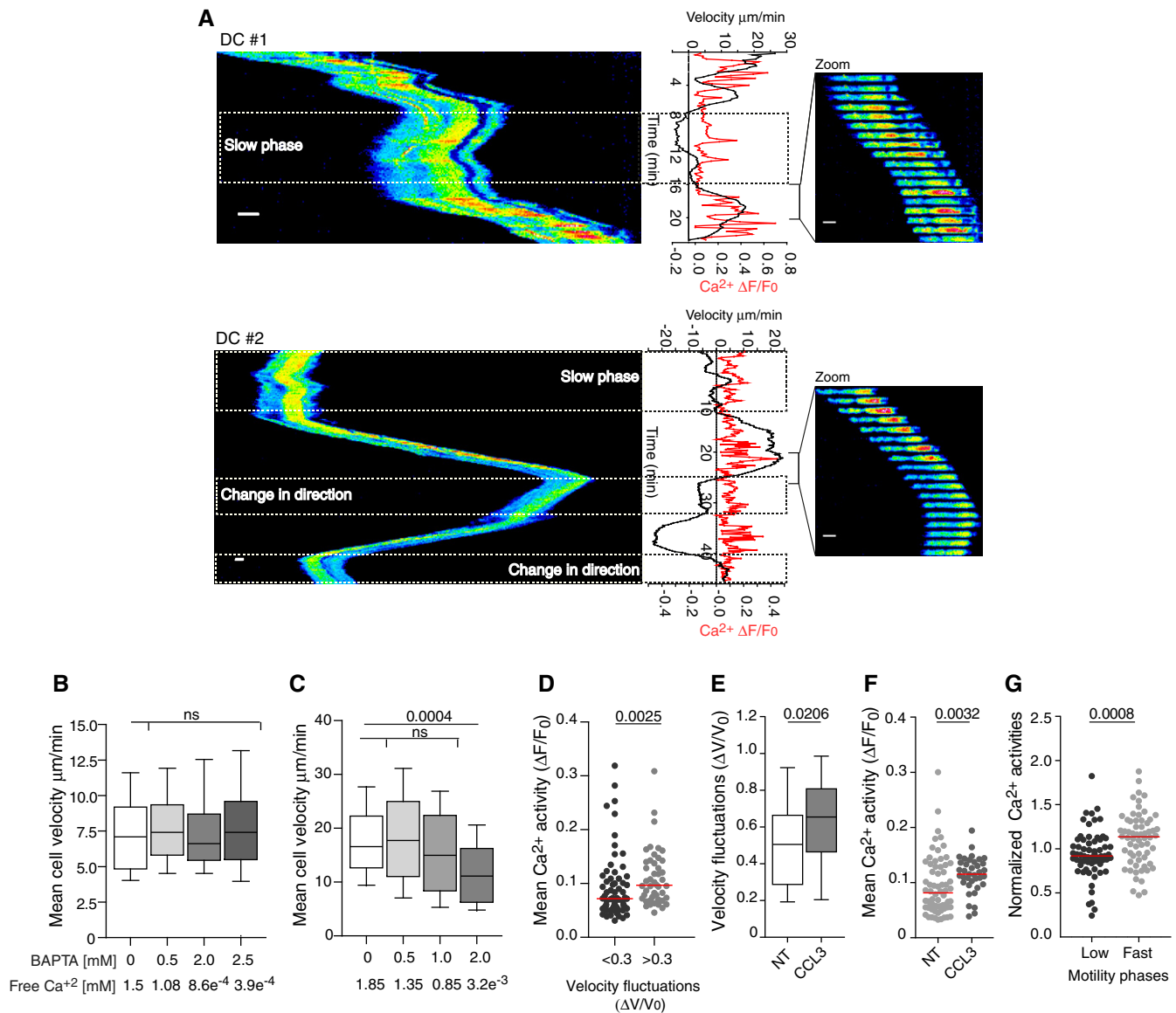
Figure 1. Ca^{2+} oscillations in immature DCs migrating in micro-channels.

A   Left, kymograph from sequential epifluorescence (20×) images showing cytosolic Ca^{2+} oscillations in speed-fluctuating immature DC after slow motility phases (upper and lower panel) and a change in direction (lower panel). DCs were loaded with the Ca^{2+} dye Oregon Green BAPTA 1-AM, introduced in micro-channels, and imaged every 10 s. Right, sequential epifluorescence (20×) images (1 image/20 s is shown). Instantaneous velocities and intracellular calcium oscillations were measured as described in Materials and Methods. Scale bar: 10 μm.

B, C   Mean cell velocity of immature DCs ($n > 125$ cells from two independent experiments) (B) or CD8$^+$ T lymphocytes ($n > 40$ cells from one experiment) (C) migrating in micro-channels with or without BAPTA. Boxes illustrate 10–90 percentiles of values, and whiskers represent the range of values. *P*-values were calculated using a Kruskal–Wallis test.

D   Mean intracellular calcium concentration in speed-fluctuating ($\Delta V/V_0 > 0.3$; $\Delta V/V_0$ relative speed variation divided by the global median velocity) and non-speed-fluctuating ($\Delta V/V_0 < 0.3$) immature DCs ($n = 187$ cells from more than three independent experiments). *P*-values were calculated using a Mann–Whitney test.

E, F   Velocity fluctuations ($\Delta V/V_0$) (E) or mean Ca^{2+} activities (F) displayed by DCs migrating in micro-channels in the presence of 100 ng/ml CCL3. *P*-values were calculated using a Mann–Whitney test, with respect to non-treated DCs (NT).

G   Mean Ca^{2+} activities during phases of fast ($> 50\%$ of max velocity) and slow ($< 50\%$ of max velocity) motility in speed-fluctuating DCs (Supplementary Fig S2F) ($n = 64$ cells, from three independent experiments). Activities were normalized to the mean Ca^{2+} activity shown by each cell during the entire movie. The *P*-value was calculated using a Mann–Whitney test.

undergoing a slow motility phase (Fig 1A upper panel) as well as in cells that changed direction upon slowing down (Fig 1A lower panel, and Supplementary Fig S2G). Altogether, these findings indicate that (i) Ca^{2+} oscillations might be specifically required for fast-migrating DCs to tune their instantaneous speed during locomotion and (ii) sustained Ca^{2+} activity may be needed for speed-fluctuating DCs to accelerate after a slow motility or an arrest phase.

Release of ER Ca^{2+} stores through IP$_3$ receptors is required to maintain intracellular Ca^{2+} levels and fast dendritic cell migration

Our data indicate that intracellular Ca^{2+} oscillations are predominantly observed during fast motility phases in speed-fluctuating DCs and that they result from Ca^{2+} release from intracellular stores rather than from extracellular Ca^{2+} influx. We therefore investigated the nature of the Ca^{2+} store(s) involved. As the endoplasmic reticulum (ER) is a major source of intracellular Ca^{2+}, we analyzed the role of IP$_3$Rs, which control the release of Ca^{2+} from the ER into the cytosol. Treatment of DCs with the IP$_3$R inhibitor xestospongin C (XestC) significantly reduced their ability to migrate in collagen-coated transwells (Supplementary Fig S3A). Similarly, the instantaneous speed of DCs crawling in micro-channels was decreased upon XestC treatment (Supplementary Fig S3B). XestC did not induce DC maturation (Supplementary Fig S3C). These data strongly suggest that IP$_3$Rs are required for immature DCs to migrate at fast speed.

DCs express all three IP$_3$R isoforms: 1, 2, and 3 (Stolk et al, 2006). To analyze their respective role in the migration of immature DCs, we silenced them individually using shRNA-encoded lentivirus. A significant reduction in IP$_3$R mRNA intracellular levels was observed by quantitative PCR upon DC infection with two shRNA-containing lentiviral particles per isoform, showing that their expression can be reduced using such strategy (Fig 2A). In the case of IP$_3$R1 and IP$_3$R3, for which specific antibodies are available, silencing was observed even more efficiently at the protein level (Fig 2B). Immunoblot and quantitative PCR analysis showed that the two shRNAs directed against IP$_3$R1 silenced both IP$_3$R1 and IP$_3$R3 isoforms, but not IP$_3$R2 (Fig 2C). The same result was obtained when using the shRNAs directed against IP$_3$R3 (Fig 2C). In contrast, the shRNAs directed against IP$_3$R2 knocked down IP$_3$R3 and IP$_3$R2 but had only a minor effect on IP$_3$R1 expression (Fig 2D). We therefore renamed these shRNAs based on their silencing specificity as following: shRNA-IP$_3$R1 = shIP$_3$R(1,3)A, shRNA-IP$_3$R2 = shIP$_3$R(2,3)B, and shRNA-IP$_3$R3 = shIP$_3$R(1,3)C. The ones highlighted in red on Fig 2E were used for the rest of our study.

None of these shRNAs triggered the activation of immature DCs (Supplementary Fig S3D, upper panels). Flow cytometry analysis of IP$_3$R-silenced DCs loaded with both Oregon Green BAPTA and FuraRed showed that they displayed strongly reduced intracellular Ca^{2+} levels as compared to control cells (Supplementary Fig S3D, lower panels). This result indicates that decreased expression of IP$_3$Rs indeed dramatically reduced the concentration of intracellular Ca^{2+}. Silencing of IP$_3$R1, 2, or 3 in immature DCs compromised their migration in collagen-coated transwells and decreased their instantaneous velocity in micro-fabricated channels (Fig 2F and G, Supplementary Fig S3E). Addition of BAPTA did not further decrease the speed of IP$_3$R-silenced DCs, indicating that the residual migration of these cells is independent of extracellular Ca^{2+} (Fig 2H). We conclude that inhibition or silencing of IP$_3$Rs impairs the migration of immature DCs.

IP$_3$ receptor 1 controls the migration persistence and space exploration capacity of immature DCs

We observed that shIP$_3$R(1,3)A and shIP$_3$R(1,3)C, which silenced both IP$_3$R1 and IP$_3$R3 but not IP$_3$R2, strongly increased speed fluctuations in immature DCs migrating in micro-channels (Fig 3A). In sharp contrast to control speed-fluctuating DCs that reached velocities below 5 μm/min, most speed-fluctuating shIP$_3$R(1,3)-silenced DCs migrated at speeds below this value (Fig 3B). This result, together with our data showing that intracellular Ca^{2+} released is mainly observed in DCs migrating at speed above 5 μm/min (Supplementary Fig S2A), supports the idea that in the absence of IP$_3$R1 and/or 3, immature DCs cannot accelerate and therefore remain in phases of slow motility. Consistent with this hypothesis, we found that the percentage of cells that changed direction during locomotion as well as the frequency of direction changes per cell were significantly enhanced in IP$_3$R1- and IP$_3$R3-silenced DCs (Fig 3C–E). Similar results were obtained when generally inhibiting IP$_3$R activity with XestC (Supplementary Fig S3F–H). Regrettably, the low intracellular Ca^{2+} levels of IP$_3$R1- and IP$_3$R3-silenced DCs did not allow us to analyze their Ca^{2+} dynamics while evolving in micro-channels (Supplementary Fig S3D, lower panels). Interestingly, no defect in DC persistence was observed when using shIP$_3$R (2,3)B, which knocked down IP$_3$R2 and IP$_3$R3 but not IP$_3$R1. Although IP$_3$R2- and IP$_3$R3-silenced DCs migrated at slower velocity (Fig 2G), they did not change direction more often as compared to control cells (Fig 3D and E). These findings suggest that IP$_3$R1, but not IP$_3$R2 and IP$_3$R3, is specifically required for immature DCs to adopt a speed-fluctuating but persistent locomotion behavior. In the absence of this molecule, DCs cannot accelerate upon slow motility phases and therefore remain in a non-persistent slow migration mode characterized by frequent changes in direction.

We therefore assessed the role of IP$_3$R1 in the migration persistence of immature DCs. For this, the migration of shIP$_3$R(1,3)A- and shIP$_3$R(1,3)C-expressing DCs was analyzed in a micro-fluidic device that confines the cells under a 5-μm-high ceiling but allows their free motion in 2D (Supplementary Fig S3I). As observed in micro-channels, both shRNAs decreased the migration speed of immature DCs in this confined 2D migration setup (Fig 4A and B). Analysis of cell individual trajectories highlighted that shIP$_3$R (1,3)A- and shIP$_3$R(1,3)C-expressing DCs exhibited constrained displacements rather than long trajectories (Fig 4C). Accordingly, quantification of their "persistence path", measured as the ratio between the effective length and the total length of the cell trajectory (Maiuri et al, 2012), showed that it was significantly decreased in these cells as compared to their control counterpart (Fig 4D). Furthermore, calculation of the "effective displacement", which corresponds to the distribution of 0- to 50-μm, 50- to 300-μm, and > 300-μm-long cell paths, indicated that shIP$_3$R(1,3)A- and shIP$_3$R(1,3)C-expressing DCs displayed shorter paths during motion as compared to control cells (Fig 4E). Equivalent results were obtained when monitoring the migration of DCs embedded in 3D collagen gels: both the migration speed and persistence were significantly decreased in IP$_3$R1,3-silenced cells (Supplementary Fig S4A–C). Together, these data indicate that (i) IP$_3$R1 controls the migration persistence of immature DCs and thus their ability to explore their surrounding space and (ii) this applies to 1D, 2D, and 3D environments. They further suggest that the velocity and persistence of DCs are two migration parameters that are differentially regulated and can be uncoupled by knocking down specific IP$_3$R isoforms.
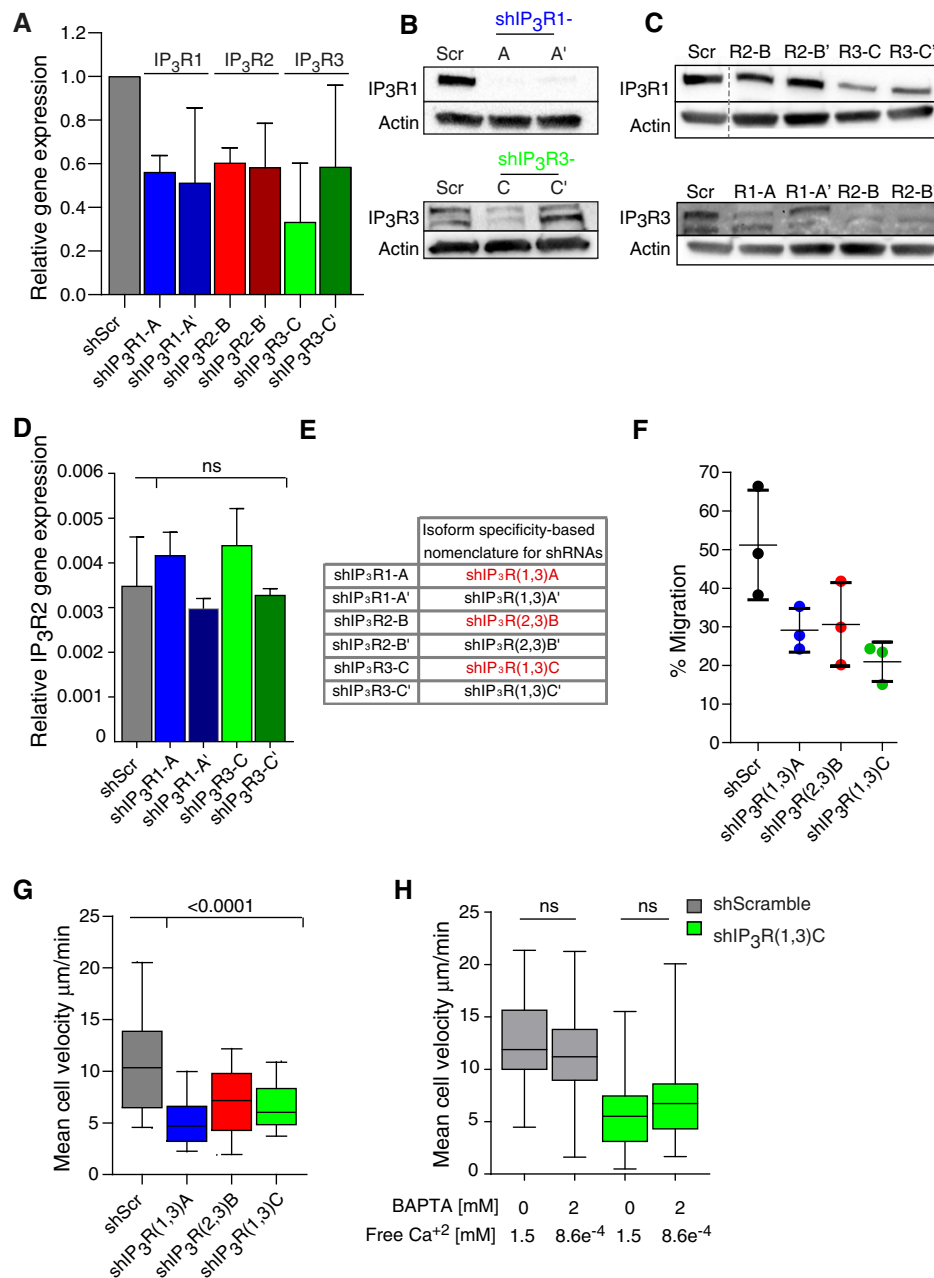
Figure 2. IP3 receptors are required for dendritic cell fast migration.

A   Relative gene expression of IP3R1 (blue), IP3R2 (red), and IP3R3 (green) in IP3R-silenced DCs. DCs were infected with two lentiviruses encoding for different shRNAs for IP3R isoforms. ShScramble-infected DCs were used as a control. Gene expression was determined by a quantitative PCR. It was calculated with respect to GAPDH expression and normalized to the levels observed in the shScramble. The median plus standard deviation of three independent experiments are shown.

B   Immunoblot for IP3R type 1 and IP3R type 3 in IP3R-silenced DCs. Actin was used as a control. IP3R3 appears as two bands as previously described (22).

C   Immunoblot for IP3R type 1 (top) and IP3R type 3 (bottom) in DCs transduced with lentivirus encoding for different IP3R shRNAs. Actin was used as a control.

D   Relative IP3R2 expression in ShScramble-infected DCs (gray), shIP3R1 (blue), and IP3R3 (green)-silenced DCs. The experiment was performed as described in (A).

E   Table showing the nomenclature for shRNAs related to their isoform-specific silencing. The shRNAs chosen to pursuit this study are highlighted in red.

F   Transmigration assay of shScramble-, IP3R(1,3)A (blue)-, IP3R(2,3)B (red)-, and IP3R(1,3)C (green)-expressing DCs. Cells were loaded in the upper chamber of a 5-μm pore collagen-coated transwell assay, recovered from the upper and lower chambers after 16 h, and counted. The median from three independent experiments is shown.

G   Quantification of the mean cell velocity of shIP3R(1,3)A (blue)-, shIP3R(2,3)B (red)-, and shIP3R(1,3)C (green)-silenced immature DCs migrating in micro-channels. shScramble-infected DCs were used as a control (gray) (*n* > 100 cells from three independent experiments for shIP3R(1,3)A and shIP3R(1,3)C and two independent experiments for shIP3R(2,3)B). Boxes illustrate 10–90 percentiles of values, and whiskers represent the range of values. *P*-values were calculated using a Kruskal–Wallis test.

H   Quantification of the mean cell velocity of shIP3R(1,3)C (green)-silenced immature DCs migrating in micro-channels in the presence of 2 mM BAPTA. shScramble-infected DCs were used as a control (gray) (*n* > 70 cells from two independent experiments). *P*-values were calculated using a Kruskal–Wallis test.

IP$_3$ receptor 1 regulates the migration of immature DCs by controlling myosin II activity and dynamics

We next searched for the mechanism by which IP$_3$R1 controls the migration persistence of immature DCs. Myosin II-mediated contractility is the main force-generating cellular component required for DC fast migration in confined environments (Faure-Andre et al, 2008; Lammermann et al, 2008). Furthermore, myosin IIA and IP$_3$R1 were shown to physically interact in MDCK cells (Hours & Mery, 2010). We therefore investigated whether myosin II

activity was altered in IP$_3$R knockdown DCs by analyzing the phosphorylation levels of its regulatory light chain MLC. Indeed, it was shown that Ca^{2+} promotes the phosphorylation of MLC by the Ca^{2+}/calmodulin-dependent MLCK, leading to motor activation and protrusion retraction in endothelial cells (Hours & Mery, 2010). MLC phosphorylation was significantly decreased in DCs transduced with the shRNAs that silenced IP$_3$R1 and IP$_3$R3 (including shIP$_3$R(1,3)A') (Fig 5A). In contrast, no MLC phosphorylation reduction was observed in cells expressing the shRNAs that silenced IP$_3$R2 and IP$_3$R3 (including shIP$_3$R(2,3)B'). This result is
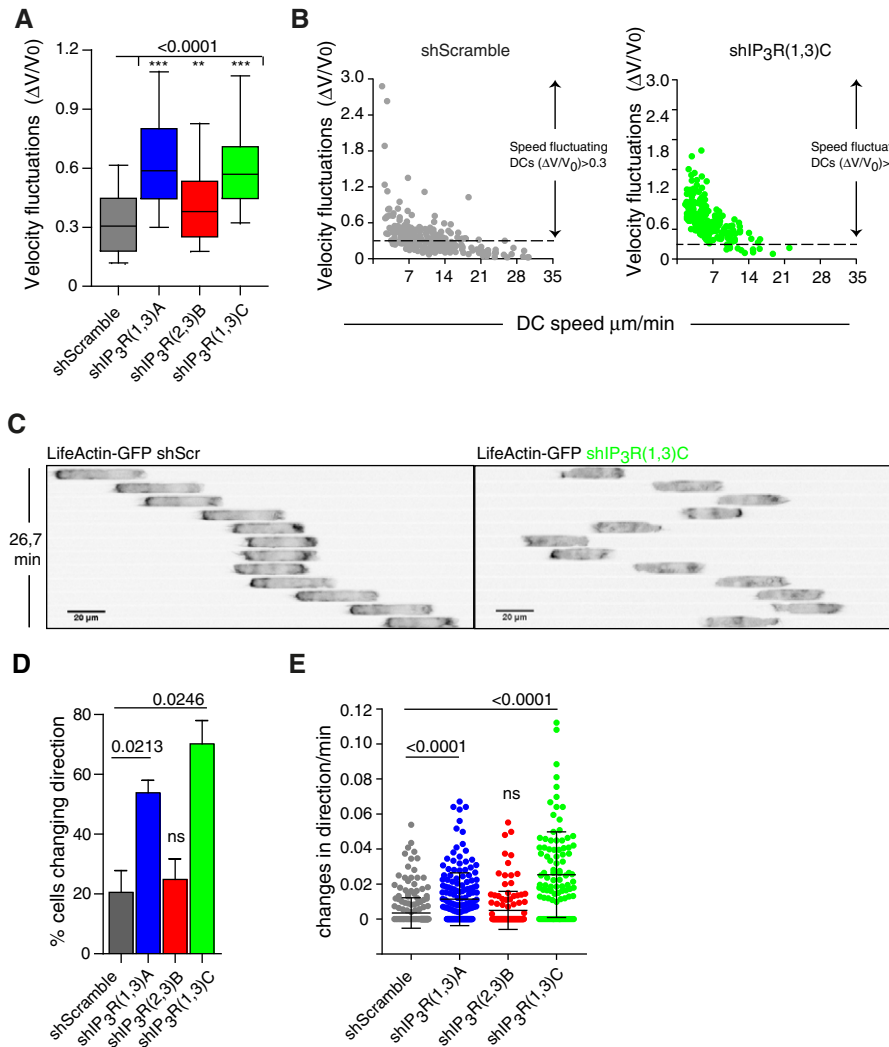

Figure 3. IP$_3$R1 silencing favors frequent changes in direction in immature DCs migrating in micro-channels.
Analysis of shScramble (gray)-, shIP$_3$R(1,3)A (blue)-, shIP$_3$R(2,3)B (red)-, and shIP$_3$R(1,3)C (green)-expressing DCs migrating in micro-channels ($n > 100$ cells per condition from 3 independent experiments for shIP$_3$R(1,3)A and shIP$_3$R(1,3)C and two independent experiments for shIP$_3$R(2,3)B).

A   Velocity fluctuations ($\Delta V/V_0$) of immature DCs migrating in micro-channels. Boxes illustrate 10–90 percentiles of values, and whiskers represent the range of values. P-values were calculated using a Kruskal–Wallis test.

B   Dot plot showing velocity fluctuations and migration speeds of shScramble (gray)- and shIP$_3$R(1,3)C (green)-expressing DCs.

C   Inverted sequential epifluorescence images (20×) of a representative control DC (left) and an immature shIP$_3$R(1,3)C-silenced DC (right) migrating in micro-channels. DCs were differentiated from LifeAct-GFP transgenic mice and imaged every 2.2 min.

D   Percentage of DCs changing their direction of locomotion while migrating in micro-channels. P-values were calculated with a paired test with respect to the shScramble condition.

E   Dot plot showing the frequency of changes in direction of immature DCs while migrating in micro-channels. Bars show the mean plus the standard deviation. A Kruskal–Wallis test was applied for statistical analysis.
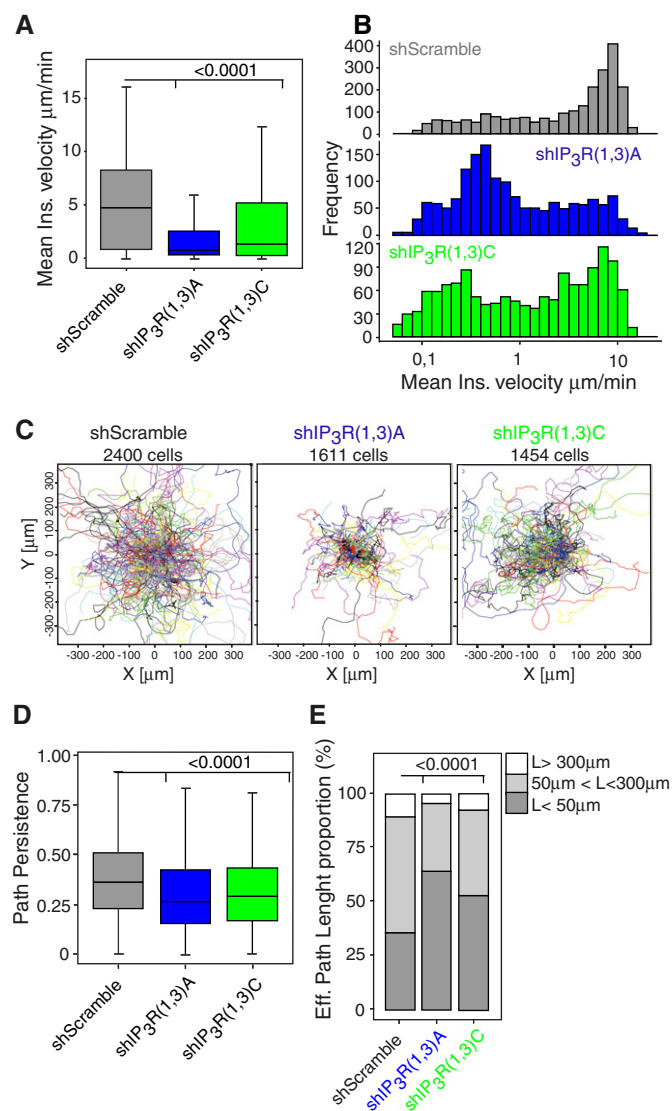
Figure 4. IP₃R1 controls the persistence of immature DCs migrating in a 2D-confined environment.

Analysis of shScramble (gray, n = 2,400 cells)-, shIP₃R(1,3)A (blue, n = 1,611 cells)-, and shIP₃R(1,3)C (green, n = 1,454 cells)-expressing DCs migrating in the device described in Supplementary Fig S3I, stained with Hoechst and imaged every 2 min during 24 h at 10× magnification. Values were obtained from three independent experiments. Cell trajectories were obtained by tracking their nucleus.

A   Graph showing the DC mean instantaneous speed. *P*-values were calculated with a *t*-test analysis.

B   Mean instantaneous speed distribution of migrating DCs.

C   Representation of individual DC trajectories.

D   Path persistence (calculated as the ratio between the effective length and the total length of the cell trajectory) of migrating DCs. *P*-values were determined with a *t*-test analysis.

E   Bars showing the proportion of the effective length displacement (L) of DCs. A Fisher's exact test (*P*-value $< 2.2 \times 10^{-16}$) was used for statistics.

consistent with shIP₃R(2,3)B not having any impact on DC velocity fluctuations and migration persistence. Of note, shIP₃R(1,3)C′ did not significantly decrease the levels of phospho-MLC, in agreement with its low silencing efficiency (Fig 2A and B). Hence, IP₃R1 is

required for myosin II activity in immature DCs migrating in confinement.

To strengthen this finding, we investigated whether myosin IIA dynamics were altered in shIP₃R(1,3)C-expressing DCs. For this, immature DCs generated from myosin IIA-GFP knock-in mice (Zhang *et al*, 2012) (the main myosin II isoform in mouse DCs; Immunological Genome project http://www.immgen.org) were imaged while migrating in micro-channels (Fig 5B and Supplementary Video S3). Myosin IIA was more abundant at the rear than at the front of migrating control DCs (Fig 5B). Inversion of this myosin IIA gradient, that is, enrichment of myosin IIA at the cell front, was associated with changes in direction in these cells (Fig 5B, star on left panel). Noticeably, myosin II dynamics were strongly altered in shIP₃R(1,3)C-expressing DCs, which changed direction even when the motor protein was mostly concentrated at the cell rear (Fig 5B, stars on right panel and Supplementary Video S3). To quantify these observations, the total myosin IIA-GFP distribution was analyzed with respect to the geometrical center of the cell (Supplementary Fig S5A) and plotted in a graph together with the speed of DCs (Fig 5C). As observed in Fig 5B, this analysis showed that when control immature DCs were moving forward (positive speed value, blue line on Fig 5C), myosin IIA was concentrated at their rear (negative value for myosin IIA distribution, red line in Fig 5C). In contrast, when their speed decreased, for example, during a change of direction, myosin IIA was found to localize at both their cell rear and front. This phase of opposition between the speed of migration and myosin IIA front/back distribution indicates that changes of direction are likely to result from strong myosin IIA enrichment at the front of control immature DCs. Strikingly, this was not observed in shIP₃R(1,3)C-expressing DCs, for which the myosin IIA distribution curve was significantly delayed with respect to the cell speed curve (Fig 5D and E). We conclude that IP₃R1 silencing alters myosin II activity and distribution so that cell directionality does not follow anymore the polarity gradient of the motor protein.

These data strongly suggest that IP₃R1 regulates the motility of immature DCs at least in part by promoting myosin IIA activity. To test this hypothesis, we analyzed DC migration in the presence of increasing amounts of the MLCK inhibitor, ML7. We found that ML7 treatment decreased the intracellular levels of active MLC in immature DCs (Fig 6A). More importantly, ML7 treatment reduced DC velocity and strongly increased their speed fluctuations and frequency of changes in direction (Fig 6B and C, and Supplementary S5B). Thus, MLCK inhibition by ML7 mimics the migratory phenotype observed in IP₃R1-silenced migrating DCs (Supplementary Fig S5C). ML7 had no effect on the migration persistence of shIP₃R(1,3) C-expressing cells (Fig 6D and E). From this result, we conclude that MLCK is most likely inactive in the absence of IP₃R1,3 and does therefore not account for the residual migration observed in IP₃R1,3-silenced DCs. Altogether, our data are consistent with a model where immature DCs use IP₃R1 and ER Ca²⁺ stores to promote the activity of myosin II and thereby maintain cell polarity during locomotion.

Discussion

We here unraveled a new role for intracellular Ca²⁺ dynamics in the regulation of amoeboid-like cell migration in confinement.
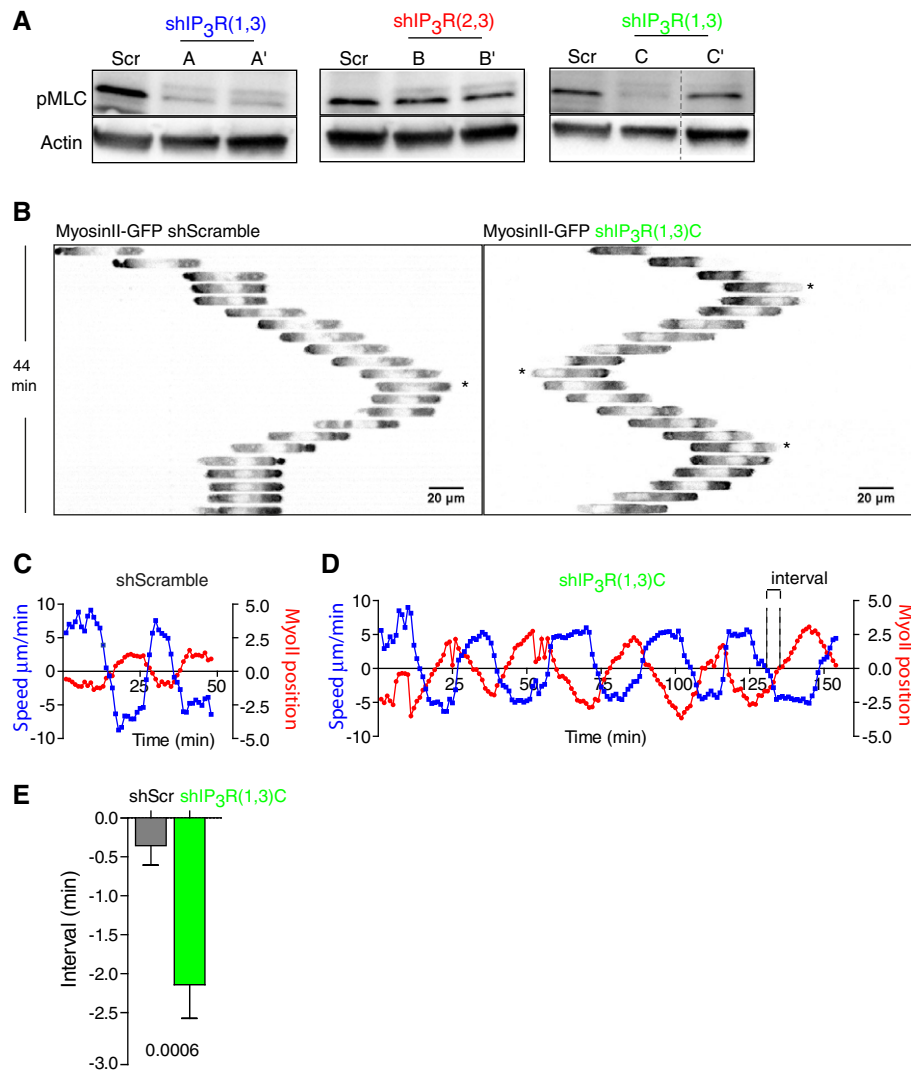
Figure 5. IP$_3$R1 regulates myosin IIA activity and dynamics in migrating immature DCs.

A   Immunoblot showing the intracellular levels of phosphorylated MLC in DCs transduced with the shScramble or shRNAs for IP$_3$Rs (shIP$_3$R(1,3)A′, shIP$_3$R(2,3)B′, and shIP$_3$R(1,3)C′). Actin was used as a control.

B   Inverted sequential epifluorescence images (20×) showing myosin IIA-GFP localization of a representative shScramble (left)- and shIP$_3$R(1,3)C-expressing DC (right) migrating in micro-channels. Myosin IIA-GFP knock-in DCs were imaged every 1 min (1 out of 2 images is shown). Asterisks highlight changes of direction during locomotion.

C, D   Myosin IIA-GFP localization (red) versus velocity fluctuations (blue, $\Delta V/V_0$) in a representative shScramble-transduced DC (C) or shIP$_3$R(1,3)C-silenced (D) migrating in micro-channels. DCs were recorded as in (B).

E   Quantification of the interval between curves (highlighted in D) obtained for myosin IIA positioning and velocity from shScramble- and shIP$_3$R(1,3)C-expressing DCs. Cells were recorded as in (B) (n = 20 cells from two experiments). The Mann–Whitney test was applied for statistical analysis.

We found that periodic intracellular Ca^{2+} increments were associated with fast motility phases in immature DCs whose speed fluctuates during locomotion. We further identified the mechanism involved by showing that inhibition of intracellular Ca^{2+} release by silencing IP$_3$R1 compromised the activity and intracellular distribution of myosin IIA, the main force-generating protein involved in fast DC migration in confinement. We propose that by maintaining an intracellular gradient of active myosin IIA, IP$_3$R1 enables DCs to tune their speed without losing their migration persistence, thereby facilitating the exploration of their environment.

Surprisingly, we found that the Ca^{2+} spikes observed in speed-fluctuating DCs occurred independently of extracellular Ca^{2+}, which was found to be dispensable for immature DC migration in micro-channels, collagen-coated transwells, and collagen gels. This unexpected result suggests that Ca^{2+} is being recycled from the cytoplasm or other intracellular stores to feed back the ER upon Ca^{2+} release. Our finding is in agreement with data showing that integrins, whose activity relies on extracellular Ca^{2+}, are not needed for DC migration in 3D environments (Lammermann *et al*, 2008). It is further reminiscent of a previous report, indicating that human polymorphonuclear cells randomly move in the presence of the
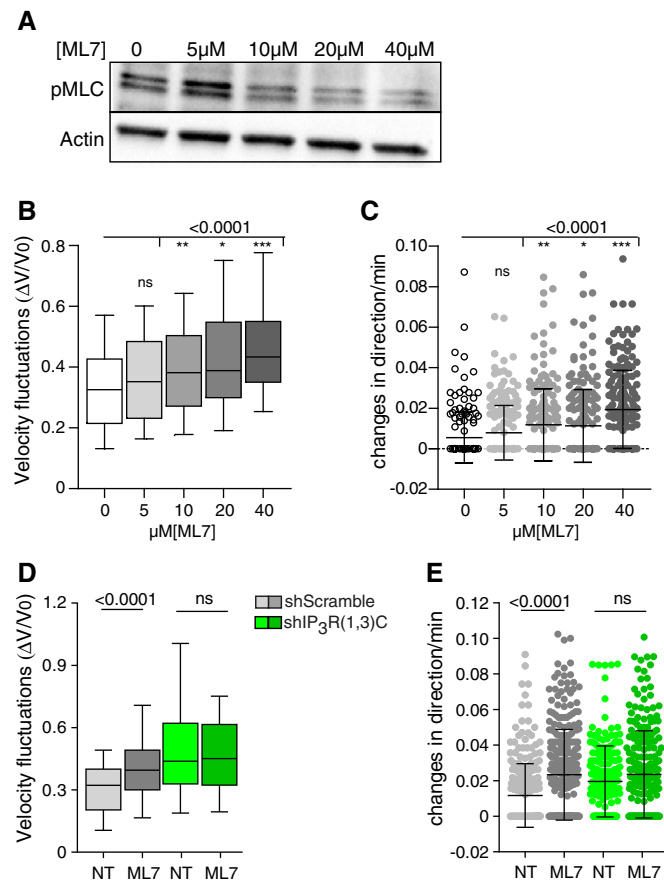
Figure 6. IP$_3$R1 controls the migration persistence of DCs through the Ca^{2+}/calmodulin-dependent myosin light chain kinase (MLCK).

A   Immunoblot showing the intracellular levels of phosphorylated MLC in DCs treated overnight with increasing amounts of the MLCK inhibitor, ML7.

B, C Analysis of immature DCs migrating in micro-channels in the presence of ML7 or DMSO as a control (*n* > 170 cells from two independent experiments). Velocity fluctuations ($\Delta V/V_0$) of immature DCs migrating in micro-channels (B). Whiskers show 10–90 percentiles plus the median. *P*-values were calculated using a Kruskal–Wallis test. Frequency of changes (C) in direction of DCs migrating in micro-channels. Mean plus SD are shown. A Kruskal–Wallis test was applied for statistical analysis.

D, E Analysis of shScramble (gray)- and shIP$_3$R(1,3)C (green)-expressing DCs migrating in micro-channels in the presence of 20 μM ML7 (*n* > 70 cells per condition from 3 independent experiments). Velocity fluctuations ($\Delta V/V_0$) of immature DCs migrating in micro-channels (D). Boxes illustrate 10–90 percentiles of values, and whiskers represent the range of values. *P*-values were calculated using a Kruskal–Wallis test. Frequency of changes (E) in direction observed in DCs migrating in micro-channels. Means plus SD are shown. A Kruskal–Wallis test was applied for statistical analysis.

Ca^{2+} chelator EDTA when squeezed between two glass slides (Malawista & de Boisfleury Chevance, 1997). This peculiar migration mode might however not apply to mature DCs, which have been shown to require extracellular Ca^{2+} influx to crawl in response to chemokine gradients (Partida-Sanchez *et al*, 2004). We have observed that LPS-matured DCs display less velocity fluctuations as well as decreased Ca^{2+} activity (MB, PV, and AMLD, unpublished results). Whether the migration of mature DCs relies on different

Ca^{2+} stores as compared to immature DCs is an interesting question that remains to be investigated.

We identified IP$_3$Rs as required to maintain intracellular Ca^{2+} levels in immature DCs migrating in confined micro-channels. Consistent with our analysis showing an association between the raise of intracellular Ca^{2+} with an increased DC locomotion, silencing of IP$_3$Rs was found to reduce their velocity, most likely by maintaining them in phases of slow motility. DCs were shown to express the three IP$_3$R isoforms, however, their role in immature DC migration was unknown (Stolk *et al*, 2006). Our results show that both IP$_3$R1,3- and IP$_3$R2,3-silenced DCs display reduced speed of locomotion, suggesting that these channels regulate DC velocity in a non-redundant manner. However, residual migration was observed in IP$_3$R1,3-silenced DCs, which might be calcium independent or involve other(s) calcium intracellular store(s). Among intracellular stores, mitochondria may be a good candidate given that these organelles were found to be polarized at the level of the uropod at the rear of amoeboid-like migrating cells (Campello *et al*, 2006), where they might promote myosin IIA contractility by locally releasing Ca^{2+}. Lysosomes have also recently emerged as important Ca^{2+} intracellular stores (Shen *et al*, 2012) and, on another hand, have been involved in the migration of phagocytes by regulating the formation of podosomes (Cougoule *et al*, 2005). Whether lysosomes regulate cell migration by allowing the release of intracellular Ca^{2+} is an intriguing possibility that could now be addressed.

Interestingly, we observed that IP$_3$R1,3-silenced DCs displayed increased velocity fluctuations and lost their migration persistence, that is, they were unable to travel over long distances for space exploration. In contrast, IP$_3$R2,3-silenced DCs did not exhibit decreased persistent migration as compared to IP$_3$R1,3-silenced DCs. In these cells, velocity fluctuations were slightly increased but most likely not enough to promote changes of migration. These results are consistent with IP$_3$R1 specifically regulating the ability of immature DCs to tune their speed during motion and modify their direction of migration. However, because this conclusion is based on shRNAs that silenced IP$_3$R1 as well as IP$_3$R3, we cannot formally exclude that these molecules show some degree of redundancy, that is, migration persistence defects might be only observed in DCs silenced for both IP$_3$R isoforms. Nonetheless, our data show that the speed and persistence of locomotion are two migration parameters that can be uncoupled in DCs. This finding is of particular interest in view of the results obtained in the first "world cell race", which showed a strong correlation between the speed and persistence of movement in a variety of cell types (Maiuri *et al*, 2012). Our study therefore suggests that the coupling between the cell migration speed and persistence is regulated at least in part by intracellular Ca^{2+} dynamics.

IP$_3$Rs work as hetero-tetramers and display different affinities for IP$_3$ binding. However, whether IP$_3$R isoforms differ in their Ca^{2+} release capacity has been a matter of debate (Patterson *et al*, 2004). Our results showing that IP$_3$R1 is required to maintain the persistence of DC migration as well as myosin II polarization and activity suggest that they might display different effector functions. A possible explanation consists in proposing that IP$_3$R1 is capable of triggering MLCK activity by releasing Ca^{2+} from the ER, whereas IP$_3$R2 and IP$_3$R3 are not, even though Ca^{2+} release is indeed reduced in IP$_3$R2- and IP$_3$R3-silenced cells. Accordingly, it was shown that

IP$_3$R1 associates with myosin IIA (Hours & Mery, 2010). IP$_3$R1 might therefore control myosin IIA activity and polarized distribution in migrating DCs by interacting with the motor protein and allowing its activation through the local release of ER Ca^{2+} stores. Such mechanism might restrict Ca^{2+} release to specific cell areas, thereby allowing the precise spatial regulation of myosin II activation during DC locomotion. Of note, treatment of IP$_3$R(1,3)-silenced DCs with the ROCK inhibitor Y27632 did not further compromise their migration persistence, indicating that this kinase does not compensate the lack of MLCK activity in these cells (PS and AMLD, unpublished results).

A question raised by this study concerns the nature of the signal (s) that trigger(s) the Ca^{2+} fluctuations observed during DC fast and persistent migration. Mechanical stimulation due to DC confinement might trigger the intracellular production of IP$_3$ and release of Ca^{2+} from the ER into the cytosol. Because DC migration *ex vivo* is strongly reduced in the absence of confinement (Heuze *et al*, 2013), it is difficult to address this question experimentally. Interestingly, myosin II itself has been involved in the generation of Ca^{2+} flickers by the stretch-activated channel TRPM7 during keratocyte chemotaxis, suggesting that mechanical forces exerted by this motor protein might be involved in intracellular Ca^{2+} release from the ER through IP$_3$Rs downstream of chemokine receptors (Wei *et al*, 2009). Importantly, TRPM7 was also shown to directly phosphorylate myosin IIA heavy chain and thereby regulate its association to actin filaments (Clark *et al*, 2008). It is tempting to speculate that activation of myosin II by confinement induces IP$_3$Rs to release ER Ca^{2+}, which in turn promotes the sustained activity of the motor protein to allow persistent DC migration through MLCK activation. Whether TRPM7 is also involved in the maintenance of myosin IIA polarized distribution and activity in migrating DCs is an opened question.

In conclusion, we here show that the release of Ca^{2+} stores from the ER through IP$_3$R1 allows immature DCs to maintain their myosin II activity and front/back asymmetry during migration independently of extracellular Ca^{2+} influx. This mechanism might enable immature DCs to efficiently explore their environment using a persistent but intermittent mode of migration, thereby optimizing their chances to find rare target antigens. How Ca^{2+} and IP$_3$ receptors regulate tissue patrolling by DCs *in vivo* shall now be addressed.

Materials and Methods

Mice and cells

Myosin IIA-GFP mice were provided by Zhang *et al* (2012). LifeAct-GFP mice were provided by M. Sixt (Riedl *et al*, 2010). Bone marrow dendritic cells were cultured during 10–12 days in medium supplemented with fetal calf serum and granulocyte–macrophage colony-stimulating factor-containing supernatant obtained from transfected J558 cells, as previously described (Faure-Andre *et al*, 2008). HEK293T cells were maintained in culture as recommended by the manufacturer (ATCC). For T lymphocyte purification and activation, mouse splenocytes were activated in the presence of 50 U recombinant interleukin-2 with 10 μl anti-CD3-/ anti-CD28-coated beads every 5–8 million cells (Miltenyi T Cell Activation/Expansion

kit, 130-093-627). After 5 days, CD8$^+$ T lymphocytes were purified from mouse spleen using a CD8a$^+$ T Cell Isolation kit II (Miltenyi, 130-095-236).

Antibodies and reagents

Micro-channels were coated with fibronectin (Sigma) or PLL(20)-g [3.5]-PEG(2) (SuSoS Chemical). For myosin light chain kinase inhibition, cells were incubated with different concentrations of ML7 from Calbiochem as indicated for 16 h. For Ca^{2+} experiments, Oregon Green BAPTA 1-AM, FuraRed, BAPTA (Invitrogen), and Thapsigargin from Calbiochem were used. For IP$_3$R inhibition, 5 μM xestospongin C from Calbiochem was used. For dendritic cell maturation, we incubate the cells 24 h with 100 ng/ml LPS (Sigma). For flow cytometry analysis, we used a homemade 24G2 anti-Fc Receptor antibodies, rabbit serum from Agro Bio as a control, and anti-CD11c (HL3 clone), anti-IAb^b (AF6-120.1 clone), and anti-CD86 (GL1 clone). For immunoblot, we used anti-IP$_3$R type 1 (Abcam ab5804), anti-IP$_3$R type 3 (610313 BD Transduction Laboratories), anti-phospho-myosin light chain (Rockland 600-401-416), and anti-actin (Millipore). For lentivirus production, HEK cells were transfected using GeneJuice (Novagen).

Preparation of micro-channels and 2D-confined devices

Micro-channels were functionalized to facilitate the diffusion of dyes and drugs (Heuze *et al*, 2011) with a final section of $5 \times 5 \times 350$ μm. They were incubated with 20 μg/ml fibronectin alone or, when indicated, with a mix of fibronectin 20 μg/ml and PLL-PEG 0.1 mg/ml at a ratio of 75/25 (vol/vol) for 1 h and washed with PBS. 2D-confined device consists of an Ø 18-mm round lamella functionalized with 5-μm-high PDMS pillars. The lamella is put over the cells plated in 12-well plates with pillars facing the cells plus a weight to squeeze them until 5 μm high. Acquisition was started after 5 h of squeezing. The lamella with micro-pillars was previously coated with 20 μg/ml fibronectin for 1 h and washed with PBS.

Analysis of intracellular Ca^{2+} levels by flow cytometry and of Ca^{2+} dynamics in migrating DCs

Free calcium concentrations were calculated using the WEBMAX Standard software (http://web.stanford.edu/~cpatton/webmaxcS. htm). For flow cytometry analysis, dendritic cells were incubated in Ringer's solution 1% BSA (in mM: 140 NaCl, 4,8 KCl, 10 glucose, 0.5 MgCl$_2$, 10 HEPES, 1 Na$_2$HPO$_4$, 1 KH$_2$PO$_4$) 30 min at 37°C and 5% CO$_2$ with 5 μM Oregon Green BAPTA 1-AM plus 5 μM FuraRed-AM. Cells were then washed in Ringer's solution and resuspended in complete media for acquisition. A ratio between Oregon Green BAPTA 1-AM and FuraRed signals was used to determine intracellular Ca^{2+} levels. For Ca^{2+} dynamics studies during DC migration, DCs were incubated with 5 μM Oregon Green BAPTA I-AM in Ringer media for 30 min, then washed and loaded in micro-channels. 2×10^5 cells were loaded in micro-channels 1 h before imaging. Images were taken every 10 s during 1–2 h. Fluorescence microscopy was performed on a Nikon TiE video microscope equipped with a cooled CCD camera (HQ2, Photometrics) using a

20× objective (NA 0.75). Image processing was performed with ImageJ software (Rasband WS. ImageJ, U.S. National Institutes of Health, Bethesda, Maryland, USA, imagej.nih.gov/ij/, 1997—2012). Cells were segmented by automatic thresholding (Yen), fluorescence intensities, and spatial coordinates of each cell were measured using the Analyze Particle plugin. Mean Oregon Green BAPTA 1-AM signals from cells were corrected to obtain $\Delta F/F_0$ ($\Delta F = F-F_0$, F_0 is the minimum signal recorded for the previous 30 frames). Velocities of cells were then estimated according to spatial coordinates. Velocity fluctuations were calculated and Ca^{2+} signal ($\Delta F/F_0$) maxima were detected. For each cell, mean Ca^{2+} signals were computed during slow (< 50% of max velocity) or fast motility phases (> 50% of max velocity). For spike frequency analysis, only calcium activities over 30% of $\Delta F/F_0$ were considered.

Velocity, changes in direction, and 2D-tracking

Cell migration analysis in micro-channels and 2D confinement was performed as described previously (Faure-Andre *et al*, 2008; Maiuri *et al*, 2012). For velocity quantification and path tracking in micro-channels, cells were loaded in micro-channels and imaged during 20 h every 1–2 min on an epifluorescence video microscope Nikon TiE microscope equipped with a cooled CCD camera (HQ2, Photometrics) using a 10× objective. Kymograph extraction and instantaneous velocity analyses were performed using a home-made program as described previously (Faure-Andre *et al*, 2008). For velocity quantification and tracking in 2D confinement, cell nuclei were stained with 200 ng/ml of Hoechst for 15 min at 37°C and cells were imaged every 2 min using a Zeiss AxioObserver microscope equipped with a 10× objective. Trajectories were determined following the fluorescent signal of the nuclei. The mean cell instantaneous speed is the mean of all instantaneous speeds of a cell. The effective length of a trajectory corresponds to the diameter of a disk that contains all the time points of the track. The cell path persistence is defined as the ratio between the effective and the total path length. Accordingly, if a cell is persistent, this value is close to one and, to the opposite, it is close to zero for a non-persistent cell.

Migration in collagen gels

DCs were mixed at 4°C with 1.6% bovine collagen type I at basic pH. Forty microliters of the mix were deposited at the center of a 35-mm glass-bottom dish, covered with a 12-mm glass slide, and incubated at 37°C during 20 min to allow fast collagen polymerization. Cells were imaged during 16 h on a video microscope (phase contrast) at a frequency of 1 image every 2 min (10× objective). To extract cell tracks, the mean image of the complete movie was subtracted to every time point, generating white objects (cells) on a dark background. Movies were processed using the FIJI plugin Filter Mean (Intensity 3) and cells tracked using a custom-made software (Maiuri *et al*, 2012).

Myosin IIA-GFP imaging and localization

For myosin II live imaging, we used DCs generated from myosin IIA HC-GFP knock-in mice and infected or not with shRNA encoded in lentiviruses. Cells were loaded in micro-channels, and myosin II HC-GFP DCs were imaged at low resolution with an epifluorescence video microscope Nikon TiE equipped with a cooled CCD camera (HQ2, Photometrics) with a 20× (NA 0.75) objective. For each cell, myosin IIA-GFP localization was measured as a vector representing the total fluorescent intensity regarding the geometrical center of the cell. The cell velocity was calculated based on the position of the geometrical center of the cell.

Lentivirus infection

For protein silencing, purified pLKO.1 lentiviral plasmids carrying shRNA sequences for IP3R1, IP3R2, and IP3R3 were obtained from Sigma-Aldrich. For shIP3R1, shRNAs #1 = TRCN0000012438, #2 = TRCN0000012439, #3 = TRCN0000012440, #4 = TRCN0000012441, and #5 = TRCN0000012442 were used. For IP3R2, shRNAs #1 = TRCN0000097136, #2 = TRCN0000277497, #3 = TRCN0000277566, #4 = TRCN0000277567, and #5 = TRCN0000097135 were used. For IP3R3, shRNAs #1 = TRCN0000012443, #2 = TRCN0000012444, #3 = TRCN0000012445, #4 = TRCN0000012446, and #5 = TRCN0000012447 were used. As control, we used an shRNA containing a scramble sequence against GFP (Cebrian *et al*, 2011).

To generate lentiviral particles, plasmids encoding lentivirus-expressing shRNAs were purified with the NucleoSpin Plasmid DNA Purification kit (Macherey-Nagel). HEK293T packaging cells were co-transfected with the transfer plasmid (pLKO/ShRNA), the pPAX2 packaging plasmid, and the pMD2G envelope plasmid (kind gifts from D. Trono, EPFL, Lausanne, Switzerland), using the GeneJuice Transfection Reagent as recommended by the manufacturer (Novagen). Virus supernatants were tittered using the QuickTiter p24 associated Lentivirus Titer kit (Cell Biolabs Inc) and used to infect day 3 DCs at a multiplicity of 0.03 pg of p24/cell by adding it directly to the culture. The medium was replaced at day 4, and infected cells were selected with 4 μg/ml puromycin from day 5 to day 7. Several washes were done during the selection process to eliminate dead cells. Infected DCs were used from day 10 to 12 for experiments.

Immunoblotting

Cells were lysed for 30 min at 4°C in a buffer containing 100 mM Tris pH 7.4, 150 mM NaCl, 0.5% NP-40, 5% glycerol, protease inhibitor cocktail, 5 mM NaF, 1 mM DTT, 1 mM Na$_3$VO$_4$, and 1 mM glycerophosphate. 30–50 μg of soluble extracts was loaded onto a 4–20% TGX gradient gel (Bio-Rad) and transferred onto a Trans-Blot Turbo PVDF/Nitrocellulose membrane (Bio-Rad). The membrane was blocked with 5% milk for 30 min, incubated with the appropriate antibodies, and revealed with SuperSignal West Dura substrate (Thermo Scientific).

Quantitative PCR

RNA extraction was done using RNA NucleSpin kit from Macherey-Nagel, and cDNA was produced from 1 μg of RNA using the Super-ScriptVILO cDNA Synthesis kit from Life Technologies. Quantitative PCR was performed using TaqMan Gene Expression Assay from Applied Biosystems. The following primers were used to analyze gene expression: Mm00439907_m1 (itpr1), Mm00444937_m1

(itpr2), Mm01306070_m1 (itpr3), and Mm99999915_g1 (gapdh) as a control.

Transmigration assays

Tissue culture-treated 96-well permeable supports (Corning 3385) were used for transmigration studies. Transwells with a 3-μm pore size membrane were coated 12 h with 5 μg/ml collagen-I and washed with PBS. 0.1×10^6 cells per well were used to perform experiments and were allowed to transmigrate during 16 h at 37°C 5% CO_2. Cells from both chambers were detached using worm PBS 5 mM EDTA and counted by flow cytometry using 10-μm beads (BioValley). The percentage of migration was determined as: % Migration = (Number of cells low chamber × 100)/(total counted cells). Propidium iodide was used to remove dead cells from the analysis.

Supplementary information for this article is available online: http://emboj.embopress.org

Author contributions

PS initiated the project on the role of IP$_3$R calcium in DC migration, designed, performed, analyzed, interpreted experiments, and participated to manuscript writing. A-ML-D directed the experimental work and wrote the manuscript. MM developed the softwares, analyzed all calcium dynamics in migrating DCs, and participated to data discussion. MLH did the CCL3, PEG calcium analysis experiments, helped design shRNA silencing experiments, and participated to data interpretation. MB did some calcium measurement experiments, helped MM with their analysis, and calculated calcium concentrations in culture media. FL helped PS with cell migration experiments in the 2D confiner and cell tracking analysis. PM wrote the softwares required to segment and analyze cell trajectories in 2D and 3D. ET helped with micro-fabrication. M-IT participated to data discussion and financially supported PS during the revision process. PL helped setting up calcium measurement experiments and participated to data discussion. MP designed migration experiments, data interpretation, and analysis together with A-ML-D. PV initiated the project on the role of calcium in DC migration, performed calcium recording experiments in 2D, analyzed the role of calcium chelation in DC and T-cell migration. Performed the migration assays in 3D collagen gels, and participated to data discussion.

Conflict of interest

The authors declare that they have no conflict of interest.

References

Barbet G, Demion M, Moura IC, Serafini N, Leger T, Vrtovsnik F, Monteiro RC, Guinamard R, Kinet JP, Launay P (2008) The calcium-activated nonselective cation channel TRPM4 is essential for the migration but not the maturation of dendritic cells. *Nat Immunol* 9: 1148−1156

Brundage RA, Fogarty KE, Tuft RA, Fay FS (1991) Calcium gradients underlying polarization and chemotaxis of eosinophils. *Science* 254: 703−706

Campello S, Lacalle RA, Bettella M, Manes S, Scorrano L, Viola A (2006) Orchestration of lymphocyte chemotaxis by mitochondrial dynamics. *J Exp Med* 203: 2879−2886

Cebrian I, Visentin G, Blanchard N, Jouve M, Bobard A, Moita C, Enninga J, Moita LF, Amigorena S, Savina A (2011) Sec22b regulates phagosomal maturation and antigen crosspresentation by dendritic cells. *Cell* 147: 1355−1368

Clark K, Middelbeek J, Lasonder E, Dulyaninova NG, Morrice NA, Ryazanov AG, Bresnick AR, Figdor CG, van Leeuwen FN (2008) TRPM7 regulates myosin IIA filament stability and protein localization by heavy chain phosphorylation. *J Mol Biol* 378: 790−803

Cougoule C, Carreno S, Castandet J, Labrousse A, Astarie-Dequeker C, Poincloux R, Le Cabec V, Maridonneau-Parini I (2005) Activation of the lysosome-associated p61Hck isoform triggers the biogenesis of podosomes. *Traffic* 6: 682−694

Faure-Andre G, Vargas P, Yuseff MI, Heuze M, Diaz J, Lankar D, Steri V, Manry J, Hugues S, Vascotto F, Boulanger J, Raposo G, Bono MR, Rosemblatt M, Piel M, Lennon-Dumenil AM (2008) Regulation of dendritic cell migration by CD74, the MHC class II-associated invariant chain. *Science* 322: 1705−1710

Guinamard R, Demion M, Launay P (2010) Physiological roles of the TRPM4 channel extracted from background currents. *Physiology* 25: 155−164

Heuze ML, Collin O, Terriac E, Lennon-Dumenil AM, Piel M (2011) Cell migration in confinement: a micro-channel-based assay. *Methods Mol Biol* 769: 415−434

Heuze ML, Vargas P, Chabaud M, Le Berre M, Liu YJ, Collin O, Solanes P, Voituriez R, Piel M, Lennon-Dumenil AM (2013) Migration of dendritic cells: physical principles, molecular mechanisms, and functional implications. *Immunol Rev* 256: 240−254

Hours MC, Mery L (2010) The N-terminal domain of the type 1 Ins(1,4,5)P3 receptor stably expressed in MDCK cells interacts with myosin IIA and alters epithelial cell morphology. *J Cell Sci* 123: 1449−1459

Knowles H, Li Y, Perraud AL (2013) The TRPM2 ion channel, an oxidative stress and metabolic sensor regulating innate immunity and inflammation. *Immunol Res* 55: 241−248

Lammermann T, Bader BL, Monkley SJ, Worbs T, Wedlich-Soldner R, Hirsch K, Keller M, Forster R, Critchley DR, Fassler R, Sixt M (2008) Rapid leukocyte migration by integrin-independent flowing and squeezing. *Nature* 453: 51−55

Lee J, Ishihara A, Oxford G, Johnson B, Jacobson K (1999) Regulation of cell movement is mediated by stretch-activated calcium channels. *Nature* 400: 382−386

Lee HC (2001) Physiological functions of cyclic ADP-ribose and NAADP as calcium messengers. *Annu Rev Pharmacol Toxicol* 41: 317−345

Lelouard H, Fallet M, de Bovis B, Meresse S, Gorvel JP (2012) Peyer's patch dendritic cells sample antigens by extending dendrites through M cell-specific transcellular pores. *Gastroenterology* 142: 592−601 e593

Maiuri P, Terriac E, Paul-Gilloteaux P, Vignaud T, McNally K, Onuffer J, Thorn K, Nguyen PA, Georgoulia N, Soong D, Jayo A, Beil N, Beneke J, Lim JC, Sim

CP, Chu YS, participants WCR, Jimenez-Dalmaroni A, Joanny JF, Thiery JP *et al* (2012) The first world cell race. *Curr Biol* 22: R673 − R675

Malawista SE, de Boisfleury Chevance A (1997) Random locomotion and chemotaxis of human blood polymorphonuclear leukocytes (PMN) in the presence of EDTA: PMN in close quarters require neither leukocyte integrins nor external divalent cations. *Proc Natl Acad Sci USA* 94: 11577 − 11582

Ng LG, Hsu A, Mandell MA, Roediger B, Hoeller C, Mrass P, Iparraguirre A, Cavanagh LL, Triccas JA, Beverley SM, Scott P, Weninger W (2008) Migratory dermal dendritic cells act as rapid sensors of protozoan parasites. *PLoS Pathog* 4: e1000222

Partida-Sanchez S, Goodrich S, Kusser K, Oppenheimer N, Randall TD, Lund FE (2004) Regulation of dendritic cell trafficking by the ADP-ribosyl cyclase CD38: impact on the development of humoral immunity. *Immunity* 20: 279 − 291

Patterson RL, Boehning D, Snyder SH (2004) Inositol 1,4,5-trisphosphate receptors as signal integrators. *Annu Rev Biochem* 73: 437 − 465

Renkawitz J, Schumann K, Weber M, Lammermann T, Pflicke H, Piel M, Polleux J, Spatz JP, Sixt M (2009) Adaptive force transmission in amoeboid cell migration. *Nat Cell Biol* 11: 1438 − 1443

Riedl J, Flynn KC, Raducanu A, Gartner F, Beck G, Bosl M, Bradke F, Massberg S, Aszodi A, Sixt M, Wedlich-Soldner R (2010) Lifeact mice for studying F-actin dynamics. *Nat Methods* 7: 168 − 169

Sallusto F, Schaerli P, Loetscher P, Schaniel C, Lenig D, Mackay CR, Qin S, Lanzavecchia A (1998) Rapid and coordinated switch in chemokine receptor expression during dendritic cell maturation. *Eur J Immunol* 28: 2760 − 2769

Shen D, Wang X, Li X, Zhang X, Yao Z, Dibble S, Dong XP, Yu T, Lieberman AP, Showalter HD, Xu H (2012) Lipid storage disorders block lysosomal trafficking by inhibiting a TRP channel and lysosomal calcium release. *Nat Commun* 3: 731

Stolk M, Leon-Ponte M, Merrill M, Ahern GP, O'Connell P (2006) IP3Rs are sufficient for dendritic cell Ca^{2+} signaling in the absence of RyR1. *J Leukoc Biol* 80: 651 − 658

Tal O, Lim HY, Gurevich I, Milo I, Shipony Z, Ng LG, Angeli V, Shakhar G (2011) DC mobilization from the skin requires docking to immobilized CCL21 on lymphatic endothelium and intralymphatic crawling. *J Exp Med* 208: 2141 − 2153

Tsai FC, Meyer T (2012) Ca^{2+} pulses control local cycles of lamellipodia retraction and adhesion along the front of migrating cells. *Curr Biol* 22: 837 − 842

Wei C, Wang X, Chen M, Ouyang K, Song LS, Cheng H (2009) Calcium flickers steer cell migration. *Nature* 457: 901 − 905

Wei C, Wang X, Zheng M, Cheng H (2012) Calcium gradients underlying cell migration. *Curr Opin Cell Biol* 24: 254 − 261

Zhang Y, Conti MA, Malide D, Dong F, Wang A, Shmist YA, Liu C, Zerfas P, Daniels MP, Chan CC, Kozin E, Kachar B, Kelley MJ, Kopp JB, Adelstein RS (2012) Mouse models of MYH9-related disease: mutations in nonmuscle myosin II-A. *Blood* 119: 238 − 250